Tikrit Journal of Engineering Sciences (2024); 31(1): 291-305
DOI: http://doi.org/10.25130/tjes.31.1.24

IRAQI Academic Scientific Journals

ISSN: 1813-162X (Print); 2312-7589 (Online)
Tikrit Journal of Engineering Sciences
available online at: http://www.tj-es.com

TJES Tikrit Journal of Engineering Sciences

The Effect of Uneven Metal Foam Distribution on Solar Compound Parabolic Trough Collector Receiver Thermal Performance

Israa S. Farhan [a,b*], *Akeel A. Mohammed* [a], *Manar S. M. Al-Jethelah* [b]

a Department of Mechanical Engineering, College of Engineering, Al-Nahrain University, Baghdad, Iraq.
b Department of Mechanical Engineering, Engineering College, Tikrit University, Tikrit, Iraq.

Keywords:
Compound Parabolic Solar Collector (CPC); Metal Foam; Pore Per Inch (PPI); Thermal Performance.

Highlights:

- *Uneven metal foam inserts distributed in the CPC receiver were investigated.*
- *PPI10 and PPI20 Cu-foam were studied.*
- *The receiver with PPI20 showed the highest temperature difference.*

ARTICLE INFO

Article history:

Received	19 Sep.	2023
Received in revised form	07 Oct.	2023
Accepted	29 Dec.	2023
Final Proofreading	03 Jan.	2024
Available online	20 Mar.	2024

Citation: Farhan IS, Mohammed AA, Al-Jethelah MSM. **The Effect of Uneven Metal Foam Distribution on Solar Compound Parabolic Trough Collector Receiver Thermal Performance**. *Tikrit Journal of Engineering Sciences* 2024; **31**(1): 291-305.
http://doi.org/10.25130/tjes.31.1.24

*Corresponding author:

Israa S. Farhan

Department of Mechanical Engineering, College of Engineering, Al-Nahrain University, Baghdad, Iraq.

Abstract: Solar energy is a key player among other renewable energies that reduce greenhouse gases and replace conventional fuel, i.e., to solve global warming and fossil fuel descending issues. However, the thermal solar systems' performance should be enhanced to cope with intermittent solar radiation. Metal foam can be used as an enhancer in solar collectors' receivers. However, metal foams are associated with pressure drop. To benefit from the metal foam as a thermal enhancer and overcome the pressure drop issue, the present study numerically and experimentally investigates a novel Compound Parabolic Solar Collector (CPC) receiver with innovative uneven metal foam inserts of varying thickness. Two pores per inch (PPI) Cu-foam inserts, PPI10 and PPI20, were tested. These inserts were strategically placed at three different positions along the receiver, with thicknesses of 3 cm, 2 cm, and 1 cm starting from the inlet side. In the experimental part, three tubular receivers were tested, empty, i.e., without metal foam, inserted with Cu-foam of PPI10, and inserted with Cu-foam of PPI20. The experiments were conducted from 09:00 AM to 04:00 PM. The investigation involved water volume flow rates from 0.2 to 0.6 l/min. The numerical part included solving the governing equations, i.e., mass, momentum, and energy conservation, simulating conditions similar to the experiments. The Brinckman model described the fluid flow through the metal foam. The thermal performance of the CPC system was evaluated using the Nusselt number (Nu), thermal efficiency, water bulk temperature, and water outlet-inlet temperature difference. Inserting Cu-foam of PPI20 resulted in the hourly maximum Nu and thermal efficiency compared to the empty and PPI10 cases. Experimentally, the hourly maximum Nu was 8.9, 8.4, and 7.9 for PPI20, PPI10, and empty receivers, respectively, at 0.6 l/min. The average thermal efficiency was 88.3, 85, and 81.9 for PPI20, PPI10, and empty receivers, respectively, at 0.6 l/min. As for the outlet-inlet water temperature difference, the highest values were at 0.2 l/min. Again, PPI20 recorded the best results, i.e., 23.3 K, 21.5 K, and 20.2 K for PPI20, PPI10, and empty cases, respectively.

تأثير التوزيع غير المتساوي لرغاوي معدنية على الأداء الحراري لمستلم مجمع شمسي مكافئ مركب

إسراء سامي فرحان[1,2]، عقيل عبدالله محمد[1]، منار صالح مهدي[2]

[1] قسم الهندسة الميكانيكية / كلية الهندسة / جامعة النهرين / بغداد – العراق.

[2] قسم الهندسة الميكانيكية / كلية الهندسة / جامعة تكريت / تكريت – العراق.

الخلاصة

تعد الطاقة الشمسية أهم أنواع الطاقة المتجددة التي تقلل من الغازات الدفيئة وتستبدل الوقود التقليدي، بمعنى آخر حل مشكلتي الاحتباس الحراري وتناقص الوقود الأحفوري. لابد من تحسين عمل أنظمة الطاقة الشمسية الحرارية للتعامل مع تذبذب الاشعاع الشمسي. يمكن استعمال رغوة معدنية كمحسن لمستلمات المجمعات الشمسية. لكن الرغوات المعدنية تكون مصحوبة بهبوط الضغط. للاستفادة من الرغوة المعدنية كمحسن حراري ومعالجة مشكلة هبوط الضغط، تدرس الدراسة الحالية عدديًا وعمليًا مركز شمسي مكافئ مركب (CPC) ذو مستقبل مبتكر مزودًا بحشوات رغوية معدنية مبتكرة ذات احجام مختلفة. تم دراسة رغوتي نحاس ذات عدد مسام لكل بوصة (PPI) ١٠ و٢٠. تم وضع هذه الحشوات بشكل استراتيجي في ثلاثة مواضع مختلفة على طول انبوب المستقبل، بسمك ١ سم، و٢ سم، و٣ سم بدء من منطقة الدخول. تضمن الجانب العملي اختبار ثلاثة أنابيب (فارغة بدون رغوة معدنية، محشوة برغوة نحاس PPI10 وآخر PPI20. أجريت التجارب العملية من الساعة ٠٩:٠٠ صباحًا ولغاية الساعة ٠٤:٠٠ عصرًا. تضمنت الدراسة معدلات تدفق حجمية للماء تتراوح من ٠,٢ إلى ٠,٦ لتر في الدقيقة. تضمن الجانب العددي حل المعادلات الحاكمة (حفظ الكتلة والزخم والطاقة)، ومحاكاة ظروف مشابهة للتجارب العملية. لوصف تدفق السوائل من خلال الرغوة المعدنية، تم استعمال نموذج برينكمان. تم تقييم الأداء الحراري لنظام CPC باستعمال رقم نسلت، والكفاءة الحرارية، ودرجة حرارة كتلة الماء خلال الانبوب، والفرق بين درجتي خروج ودخول الماء. حشو رغوة نحاس (PPI20) نتج عنه أعلى رقم نسلت ساعي وكفاءة حرارية مقارنة بالمستلم الفارغ والمستلم المحشو برغوة نحاس بـ(PPI10). عمليًا كان أعظم رقم نسلت ساعي ٨,٩ و٨,٤ و٧,٩ لـPPI20 وPPI10 والمستلم الفارغ على التوالي عند ٠,٦ لتر/دقيقة. متوسط الكفاءة حرارية كان ٨٨,٣ و٨٥ و٨١,٩ لـPPI20 وPPI10 والمستلم الفارغ على التوالي عند ٠,٦ لتر/دقيقة. بالنسبة لفرق درجتي حرارة الخروج والدخول فكانت أعظم قيم عند ٠,٢ لتر/دقيقة. مرة أخرى سجلت PPI20 أفضل النتائج (٢٣,٣ كلفن و٢١,٥ كلفن و٢٠,٢ كلفن لكل من PPI20 وPPI10 والمستلم الفارغ على التوالي).

الكلمات الدالة: مركز شمسي مكافئ مركب (CPC)، رغوة معدنية، عدد المسام لكل بوصة (PPI)، أداء حراري.

1.INTRODUCTION

The increasing need for sustainable energies, particularly solar energy, has been driven by several factors, including the depletion of fossil fuel supplies, their detrimental impact on the environment, and their rising costs. The sun is the primary provider of many forms of energy on Earth, notably solar and wind energies [1]. Numerous applications, such as producing hot water, heating spaces, and cooling [2], may employ solar energy. The significant interest in these applications is the thermal energy converted from solar energy. The solar irradiation can be converted into thermal heat using the thermal solar collectors [3–5]. In a thermal solar collector, the solar irradiation is absorbed in its absorber and converted into thermal energy, i.e., heat. The produced heat then convects to a working fluid, such as water, air, or oil. Besides directly utilizing the produced thermal energy in heating spaces or water, the produced thermal energy can be stored in phase change materials, for instance. This stored thermal energy can be used when the solar insolation is low as in cloudy or dusty days or absent at night. Solar thermal collectors are classified into concentrating and non-concentrating collectors [6]. Concentrating solar collectors generate non-pullulated thermal energy, enhance collector performance, and reduce the production of thermal energy costs. One of the concentrating collectors' types is the compound parabolic concentrator (CPC). CPC is a linear concentrating collector with a concentration ratio ranging from 1 to 5. The CPC's receiver is usually a tube rounded be evacuated tubular glass cover. The CPC produces high-temperature working fluid. The CPC collector can be operated with or without tracking systems. The stationary CPC collectors, i.e., non-tracking, are cost-effective systems [7]. Enhancing the concentrating collectors' performance has been considerably studied by many researchers [8]. One significant thermal enhancement is using metal foams. A metal foam consists of interconnected cells and metal ligaments; therefore, it causes flow mixing, has a high surface area-to-volume ratio, and low density [9]. The common commercial metal foam materials are aluminum, copper, steel, ceramics, and nickel. A metal foam is characterized by its pores and struts diameters. Duan [10] investigated the effect of aerogel on the performance of flat-plate collector. The aerogel was fixed between the absorber and the cover. Using the aerogel significantly enhanced the collector's thermal efficiency by 1.66 times the traditional collector. Chen and Huang [11] numerically studied the impact of aluminum alloy blocks on a flat-plate solar collector. The aluminum alloy foam blocks were with varying porosities ($0.85 < \varepsilon \leq 0.95$) and pore per inch (PPI) values ranging from 5 to 40. These foam blocks were individually fixed below the absorber. The authors found that the aluminum foam blocks significantly increased the average Nusselt number up to six times than without the aluminum foam. Ali and Ghashim [12] numerically investigated the heat transfer characteristics of a horizontal pipe filled with porosity metal foam (ε= 0.9) under uniform heat flux. They conducted three-dimensional simulations for four cases with various pores per inch (PPI) of copper foams (10, 20, 30, and

40). The Nusselt number ratio increased with the pore density of the metal foam, and the increase was higher for higher PPI metallic foams. The pressure drop in the pipe was higher for higher PPI metallic foams, increasing flow resistance. However, the pressure drop decreased when the copper foam was only partially filled in the middle of the pipe. Forced convective heat transfer in a solar water collector channel with three aluminum metal-foam blocks (ε = 0.85, 0.9, and 0.95) attached to the internal wall was numerically studied by Albojamal [13]. The results showed that the Darcy number had a significant role in improving heat transfer. Furthermore, it has been found that interactions between the fluid and the first porous block produced the majority of the augmentation. Hence, using a one-block reduced the pumping power. The investigated configurations exhibited a maximum thermal enhancement as the Nusselt number increased three times more than the without blocks scenario. Ranjithkumar et al. [14] experimentally investigated the advantages of integrating a flat-plate solar air heater with a porous material under Indian climate conditions. The porous media employed in the study consisted of black stone and sandstone. The stones were additionally employed as a heat-storing medium. The results showed that incorporating the porous medium improved the air heater efficiency. The efficiency was 50% and 63.3% using black stone and sandstone, respectively, at 0.03 kg/s air mass flow rate. Jamal-Abad [15] experimentally investigated the impact of a partially porous medium, i.e., copper (ε = 0.9, PPI=30), in the absorber of a parabolic trough collector on the collector efficiency. Adding the partial porous increased the pressure drop and decreased the overall heat loss coefficient by 45%, increasing the system's efficiency. Valizade et al. [16] experimentally three cases of the porous medium (ε = 0.95, PPI=10): fully, semi-, and without a porous medium. It was found that the maximum temperature difference between the outlet and inlet were 12.2°C, 8.8°C, and 3.3°C for fully, semi-, and without porous medium. The system's thermal efficiency increased by 171.2% and 119.6% using fully and semi-porous medium compared to the non-porous case. Heyhat and Khattar [17] experimentally studied the impact of placing porous medium (ε = 0.95, PPI=10 and 20) in the absorber on a parabolic trough solar collector's thermal efficiency. The highest thermal efficiencies were obtained for the full, at the center, and on the perimeter, i.e., 50.8%, 46.1%, and 44.7%, respectively. The peripheral placement showed lower thermal efficiency and pressure drop than placing the porous medium in the absorber center. Saedodin et al. [18] numerically and experimentally studied the impact of adding porous medium (ε = 0.93, PPI= 20) in a flat-plate collector. The Nusselt number increased up to 82% using the porous medium. However, the pressure drop increased. Peng et al. [19] numerically and experimentally studied the impact of a semi-annular porous medium with triangular, rectangular, and trapezoidal fins on the parabolic trough collector's performance. The results showed that such a design increased the Nusselt number, friction factor, and performance evaluation criteria to 383.7%, 788.8%, and 360%, respectively. The triangular fins resulted in better thermodynamic and thermohydraulic performance than the trapezoidal and rectangular fins. The previous studies investigated the performance of parabolic solar collectors inserted with the same size of porous foam. They indicated an improvement in the thermal performance of the solar collectors as metal foam was inserted. However, they also indicated an increase in the pressure drop associated with inserting metal foams. The studies on compound parabolic solar collectors are less than parabolic. Also, the uneven distribution and sizes of metal foam inserts have yet to be studied. Such an arrangement could improve the thermal performance of the solar collector with less pressure drop through the receiver. This study studied a novel compound parabolic solar collector (CPC) receiver with metal foam inserts with gradually increasing thicknesses along the CPC receiver. Three compound parabolic solar collectors were designed and fabricated to study the collector's thermal performance. One CPC receiver was empty as a reference. The second CPC receiver was inserted with three uneven copper metal foam with PPI20. The third CPC receiver was inserted with three uneven copper metal foam with PPI10. The Nu number, bulk temperature, and thermal efficiency of receiver tubes in the three cases have been analyzed and compared.

2.MATHEMATICAL MODEL

A three-dimensional model in a cylindrical coordinate system describes the problem of unsteady mixed convection heat transfer in an absorber tube receiver in the horizontal position. Two models were built: one without metal foam and the other with metal foam insertion. The second model includes an absorber tube receiver partially filled with discrete metal foams in descending order and peripherally heated uniformly by solar radiation. The absorber wall is impermeable and rigid.

2.1.The Governing Equations

This study introduced the conservation of mass, conservation of momentum Navier-Stokes equations, and conservation of energy to describe the 3-D flow field in the clear fluid region. While the volume-averaged generalized momentum equation, i.e., the Brinkman-

extended Darcy model, is introduced to describe the flow field inside the porous medium. Since the absorber was symmetry, the governing equations and terms in the θ-direction were neglected. The following assumptions were applied: the flow was hydrodynamically fully developed laminar, the fluid was incompressible and single phase, the heat transfer fluid was Newtonian fluid and followed Boussinesq's Approximation, unsteady state, the absorber pipe was smooth and with the no-slip condition at the pipe wall, no heat generation or dissipation, the metal foam was rigid, uniform, isotropic, and fully saturated with water, local thermal equilibrium, the absorber pipe and metal foam thermophysical properties were constant. Based on the above assumptions, the equations mentioned above are expressed as follows [20]:

Continuity equation

$$\frac{1}{r}\frac{\partial(rU_r)}{\partial r}+\frac{1}{r}\frac{\partial U_\theta}{\partial \theta}+\frac{\partial U_z}{\partial z}=0 \quad (1)$$

Momentum equation in fluid in the r-direction:

$$\left(\frac{\partial U_r}{\partial t}+U_r\frac{1}{r}\frac{\partial(rU_r)}{\partial r}+\frac{U_\theta}{r}\frac{\partial U_r}{\partial \theta}-\frac{U_\theta^2}{r}+U_z\frac{\partial U_r}{\partial z}\right)=-\frac{1}{\rho}\frac{\partial P}{\partial r}+\vartheta\left(\frac{\partial}{\partial r}\left(\frac{1}{r}\frac{\partial(rU_r)}{\partial r}\right)+\frac{1}{r^2}\frac{\partial^2 U_r}{\partial \theta^2}-\frac{2}{r^2}\frac{\partial U_\theta}{\partial \theta}+\frac{\partial^2 U_r}{\partial z^2}\right)+g[1-\beta(T-T_0)]\cos\theta \quad (2)$$

Momentum equation in the θ-direction

$$\left(\frac{\partial U_\theta}{\partial t}+U_r\frac{\partial U_\theta}{\partial r}+\frac{U_\theta}{r}\frac{\partial U_\theta}{\partial \theta}+\frac{U_rU_\theta}{r}+U_z\frac{\partial U_\theta}{\partial z}\right)=-\frac{1}{\rho}\frac{1}{r}\frac{\partial P}{\partial \theta}+\vartheta\left(\frac{\partial}{\partial r}\left(\frac{1}{r}\frac{\partial(rU_\theta)}{\partial r}\right)+\frac{1}{r^2}\frac{\partial^2 U_\theta}{\partial \theta^2}+\frac{2}{r^2}\frac{\partial U_r}{\partial \theta}+\frac{\partial^2 U_\theta}{\partial z^2}\right) \quad (3)$$

Momentum equation in the z-direction:

$$\left(\frac{\partial U_z}{\partial t}+U_r\frac{\partial U_z}{\partial r}+\frac{U_\theta}{r}\frac{\partial U_z}{\partial \theta}+U_z\frac{\partial U_z}{\partial z}\right)=-\frac{1}{\rho}\frac{\partial P}{\partial z}+\vartheta\left(\frac{1}{r}\frac{\partial}{\partial r}\left(r\frac{\partial U_z}{\partial r}\right)+\frac{1}{r^2}\frac{\partial^2 U_z}{\partial \theta^2}+\frac{\partial^2 U_z}{\partial z^2}\right) \quad (4)$$

The energy equation

$$\left(\frac{\partial T}{\partial t}+U_r\frac{1}{r}\frac{\partial(rT)}{\partial r}+\frac{U_\theta}{r}\frac{\partial T}{\partial \theta}+U_z\frac{\partial T}{\partial z}\right)=\alpha\left[\frac{1}{r}\frac{\partial}{\partial r}\left(r\frac{\partial T}{\partial r}\right)+\frac{1}{r^2}\frac{\partial^2 T}{\partial \theta^2}+\frac{\partial^2 T}{\partial z^2}\right] \quad (5)$$

For modeling heat transfer and fluid flow in the metal foam domain, the Brinkman-extended Darcy equation with local thermal equilibrium was used [21-23].

Momentum equation in the r-direction:

$$\frac{\rho}{\varepsilon^2}\left(\frac{\partial U_r}{\partial t}+U_r\frac{1}{r}\frac{\partial(rU_r)}{\partial r}+\frac{U_\theta}{r}\frac{\partial U_r}{\partial \theta}+\frac{U_\theta^2}{r}+U_z\frac{\partial U_r}{\partial z}\right)=-\frac{\partial P}{\partial r}-\frac{\mu}{K}U_r+\frac{\mu}{\varepsilon}\left[\frac{\partial}{\partial r}\left(\frac{1}{r}\frac{\partial(rU_r)}{\partial r}\right)+\frac{1}{r^2}\frac{\partial^2 U_r}{\partial \theta^2}-\frac{2}{r^2}\frac{\partial U_\theta}{\partial \theta}+\frac{\partial^2 U_r}{\partial z^2}\right] \quad (6)$$

Momentum equation in the θ-direction:

$$\frac{\rho}{\varepsilon^2}\left(\frac{\partial U_\theta}{\partial t}+U_r\frac{\partial U_\theta}{\partial r}+\frac{U_\theta}{r}\frac{\partial U_\theta}{\partial \theta}+\frac{U_rU_\theta}{r}+U_z\frac{\partial U_\theta}{\partial z}\right)=-\frac{1}{r}\frac{\partial P}{\partial \theta}-\frac{\mu}{K}\frac{1}{r}U_\theta+\frac{\mu}{\varepsilon}\left[\frac{\partial}{\partial r}\left(\frac{1}{r}\frac{\partial(rU_\theta)}{\partial r}\right)+\frac{1}{r^2}\frac{\partial^2 U_\theta}{\partial \theta^2}+\frac{2}{r^2}\frac{\partial U_r}{\partial \theta}+\frac{\partial^2 U_\theta}{\partial z^2}\right] \quad (7)$$

Momentum equation in the z-direction:

$$\frac{\rho}{\varepsilon^2}\left(\frac{\partial U_z}{\partial t}+U_r\frac{\partial U_z}{\partial r}+\frac{U_\theta}{r}\frac{\partial U_z}{\partial \theta}+U_z\frac{\partial U_z}{\partial z}\right)=-\frac{\partial P}{\partial z}-\frac{\mu}{K}U_z+\frac{\mu}{\varepsilon}\left[\frac{1}{r}\frac{\partial}{\partial r}\left(r\frac{\partial U_z}{\partial r}\right)+\frac{1}{r^2}\frac{\partial^2 U_z}{\partial \theta^2}+\frac{\partial^2 U_z}{\partial z^2}\right] \quad (8)$$

The energy equation

$$\frac{\partial T}{\partial t}+U_r\frac{1}{r}\frac{\partial(rT)}{\partial r}+\frac{U_\theta}{r}\frac{\partial T}{\partial \theta}+U_z\frac{\partial T}{\partial z}=\alpha_{\text{eff}}\left[\frac{1}{r}\frac{\partial}{\partial r}\left(r\frac{\partial T}{\partial r}\right)+\frac{1}{r^2}\frac{\partial^2 T}{\partial \theta^2}+\frac{\partial^2 T}{\partial z^2}\right] \quad (9)$$

where α_{eff} is the effective diffusivity in (m²/s) [24]:

$$\alpha_{eff}=\frac{k_{eff}}{(\rho C_P)_f} \quad (10)$$

3.NUMERICAL MODEL

The present study is intended to solve the governing equations of flow through a compound parabolic trough absorber using the COMSOL Multiphysics 5.4a® software program. The Galerkin Finite Element Method (FEM) was utilized to solve the physical problem. The Galerkin method transforms the continuous functions to a weak form, i.e., multiply the weighting functions with differential problems, then integrate them by parts over the studied domain. The numerical results were obtained under a convergence order of 10^{-5}. The present analysis investigates the influences of metal foam on the heat and fluid flow patterns and heat transfer rate inside the absorber. The following models were studied:

1. Model (I): An absorber of CPC without a metal foam, see Fig. 1.
2. Model (II): An absorber of CPC with descending order of metal foam. The studied metal foam was copper, i.e., porosity of 95% and PPI 10 and 20, see Fig. 1. The thermophysical properties of copper are listed in Table 1. The specifications of the studied model are listed in Table 2.

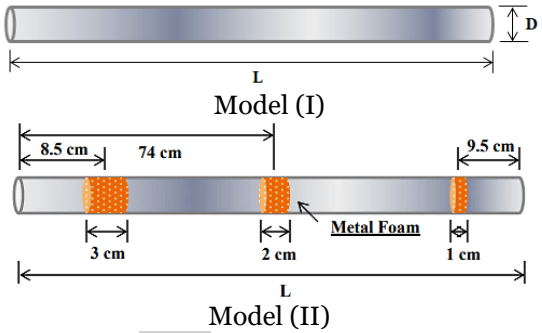

Fig. 1 Studied Models

Table 1 Copper Thermophysical Properties.

Parameter	Copper
Density (kg/m³)	8933
Thermal Conductivity (W/m °C)	401
Specific Heat Capacity (J/kg.°C)	385

Table 2 The Studied Modeled Specifications.

Item	Details
Absorber length	150 (cm)
Absorber diameter	1 in (2.54 cm)
Metal foam length	3 (cm), 2 (cm), and 1 (cm)
Metal foam diameter	1 in (2.54 cm)
Metal foam porosity	95%
Metal foam PPI	10 and 20
Metal foam material	Copper

3.1.Grid Generation and Independence

A 3-D circular pipe of length 150 cm and a diameter of 2.54 cm without/with metal foam was numerically investigated. The flow and heat transfer inside the pipe were simulated. After applying the required physics, i.e., the Brinkman equation to describe the fluid flow and heat transfer in fluids with porous medium physics, the pipe was discretized into elements, i.e., mesh. The tetrahedron mesh type was selected due to its flexibility and accurate representation of the curved surfaces. Fig.2 shows the mesh geometry of the studied pipe. The grid independence should be tested to avoid the grid size effect on the results. The grid independence test was performed for the following conditions: uniform heat flux at the absorber surface= 900 W/m^2, inlet temperature= 303.1 K, and the mass flow rate at the absorber inertance= 0.007 kg/s. The mesh independency test results are shown in Table 3. A range of number of elements from 25,383 to 280,048 was tested. The results for lower elements number resulted in non-reasonable outcomes. More elements produced a huge number of degrees of freedom, causing a crash for the laptop. The differences between the third and fourth cases were 0.003%, 0.003%, 0.71%, and 0.018% for the outlet temperature, friction factor, Nusselt number, and efficiency, respectively. The number of elements of 146,570 was considered because beyond that the outcomes slightly change and to make a trade-off between the outcomes' accuracy and the CPU time.

Table 3 Mesh Independency Test.

Case	Number of Elements	T_{out} (K)	f	Nu	η
1	25,383	305.793	0.22940	5.75	69.22
2	49,142	305.734	0.22931	6.5	67.70
3	146,570	305.723	0.22929	7	67.42
4	280,048	305.722	0.22930	7.05	67.43

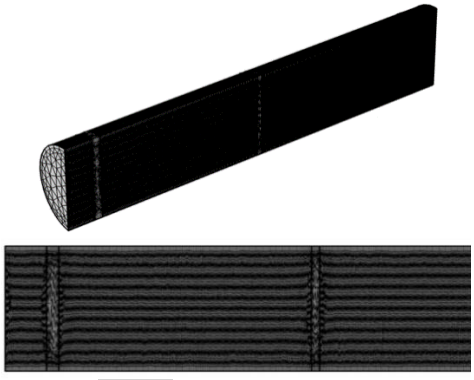

Fig. 2 Mesh Geometry.

4.EXPERIMENTAL VALIDATION

4.1.Experimental Setup

This study introduces a novel design for a compound parabolic solar collector (CPC) receiver, as shown in Fig.3. Incorporating copper foam inserts with progressively reducing thicknesses along the length of the CPC receiver. The experimental configuration consisted of a compound parabolic reflector with an acceptance angle of 47°, combined with a galvanized steel pipe with an inner diameter of 0.0254 m and a length of 1.5 m. To mitigate the reflection of the receiver pipe, it was covered with a matte black substance. The reflector and receiver pipe were in a wooden enclosure topped with a 4-mm glass plate. The enclosed area within the box was subjected to air evacuation to minimize heat transfer through convection from the receiver to the surrounding environment. Water was utilized as the heat transfer fluid. A storage tank was linked to the CPC to supply it with water, and the water discharged from the CPC was afterward directed into the tank. To facilitate the water movement throughout the investigated system, a small pump (CRS25/4-180) was mounted before the absorbers entrance, continuously circulating the water in the present system. The studies were conducted between May and June 2023, between 09:00 AM and 04:00 PM. To ensure the reliability of the findings, the experiments were repeated three times, each yielding consistent results. Five volumetric flow rates were examined, specifically 0.2, 0.3, 0.3, 0.4, 0.5, and 0.6 l/min. The selected flow rates were intended to ensure that the flow through the receiver was fully developed.

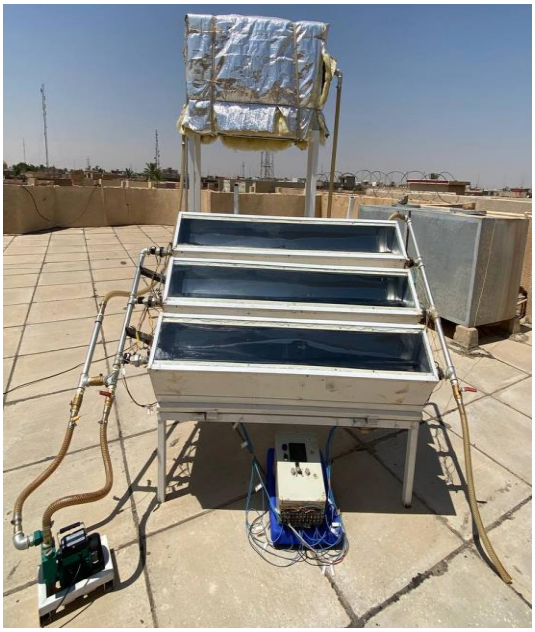

(a)

(b)

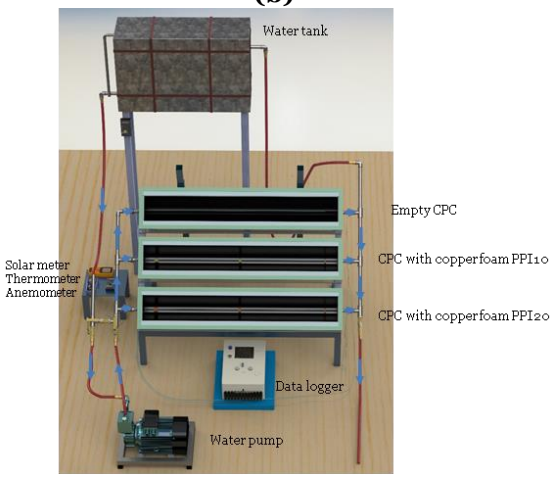

(c)

Fig. 3 The Novel CPC System (a) Front View, (b) Side View, and (c) Schematic Diagram.

The study examined one type of metal foam, i.e., copper. Two pores per inch (PPI) values, 10 and 20, as shown in Fig. 4, were examined for each metal foam alongside an empty receiver utilized as a reference. Three metal foam inserts were positioned 10 cm from the receiver inlet, in the center of the receiver, and 10 cm from the receiver outlet.

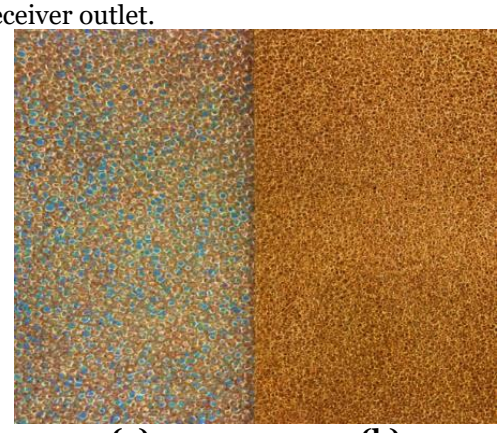

(a) **(b)**

Fig. 4 Copper Metal Foam with Fixed Porosity 0.95: (a) PPI10, (b) PPI20.

The thicknesses of the implants were distributed as follows: 3 cm, 2 cm, and 1 cm, respectively, as shown in Fig. 5. The flow meter (Arduino UNO, YF-S201) was used to measure the flow rate of the flowing water. Nine thermocouples were arranged at the top surfaces of the absorber tubes with and without a metal foam. Six K-type-thermocouples (with a precision of ±0.1 °C) were inserted into the flow at the inlet and outlet of tested tubes to measure the temperature of the water. Two thermocouples were used to measure the glass cover and ambient temperature. Six pressure transducers (Arduino UNO, G1/4) were installed at the inlet and outlet of the test tubes to measure the pressure drop. The solar radiation was measured using a Solar Power Meter SM206. Also, a small pump (CRS25/4-180) was mounted before the absorbers entrance, which continuously circulated the water through the present system.

PPI20

PPI10

Fig. 5 Distribution of Copper Foam Inserts Inside the Absorber Tube.

4.2.Data Analysis

4.2.1.The Thermal Analysis of Compound Parabolic Collectors

The compound parabolic collector thermal performance is expressed using the following data reduction equations. The absorbed radiation, S, is obtained from [25]:

$$S = G_t \tau_g \alpha_r \tau_{CPC} \quad (11)$$

Effective transmissivity of CPC, which can be expressed as:

$$\tau_{CPC} = \rho^n \quad (12)$$

The collector efficiency factor (F′) is the useful energy to the maximum possible useful energy. F′ indicates the heat transfer portion from the receiver to the working fluid. It can be calculated from Eq. (13):

$$F' = \frac{\dot{m}\, c_p(T_o - T_i)}{A_a[S - U_L(T_m - T_a)]} \quad (13)$$

The useful energy gain can be calculated from:

$$Q_u = F' A_a[S - U_L(T_m - T_a)] \quad (14)$$

The collector efficiency is given by:

$$\eta = \frac{Q_u}{A_c\, G_t} \quad \textbf{(15)}$$

4.2.2.Heat Transfer and Fluid Flow Analysis in the Receiver

In the receiver, the heat transfers from the receiver wall to the heat transfer fluid by convection. The local Nusselt number in the receiver can be expressed as:

$$Nu_z = \frac{h_z D_h}{k} \quad \textbf{(16)}$$

Where the local convection heat transfer coefficient (h_z) is calculated from:

$$h_z = \frac{Q_u}{A_p(T_r - T_i)} \quad \textbf{(17)}$$

The average Nusselt number is defined as:

$$Nu = \frac{1}{L}\int_0^L h_z\, dz \quad \textbf{(18)}$$

4.3.The Uncertainty Analysis

The measurement system consisted of a chain of components; each has an individual accuracy. The uncertainties of experimental quantities were estimated using the method presented by Kline and McClintock [26]. Hence, the experimental errors that may happen in the independent parameters are given in Table 4, which is taken from measuring devices as follows:

Table 4 The Uncertainties of Experimental Quantities.

Independent parameter (e)	Uncertainty (W)
K-type thermocouples	±0.3 °C
Solar radiation (G_t)	± 5 W/m2
Mass flow rate (ṁ)	±0.0008 kg/s
Pressure drop (ΔP)	± 0.001 Pa

5.RESULT AND DISCUSSION

5.1.Weather Condition

Fig. 6 displays the variations in solar radiation intensity from 09:00 AM to 04:00 PM for the selected test days in May and June. Notably, a consistent pattern is observed in solar radiation throughout the day for these dates. The data indicates that the solar radiation intensity gradually increased as the day progressed. The highest solar radiation was usually at 12:30 PM for the tested days. The solar radiation intensity declines after achieving its maximum value at 12:30 PM. This decline continued as the afternoon unfolded, eventually reaching a low point at 04:00 PM when the data collection period ended. Fig. 7 depicts ambient temperature variations over the experimental period. Fig. 7 shows a direct relationship between the ambient air temperature and solar radiation intensity. As solar radiation intensity increased, the ambient temperatures also increased. However, an interesting phenomenon occurred later in the day. After 01:00 PM, a delayed decline in the ambient air temperature was observed, even as the solar radiation intensity decreased. This delay is attributed to the thermal energy retained in the surrounding buildings and environment throughout the day, which continued to release heat into the ambient air post-solar noon.

5.2.Nusselt Number

5.2.1.Impact of Metal Foam PPI on the Hourly Nusselt Number

Copper Metal Foam Inserts with fixed porosity (0.95) and varying pores per inch (PPI) values of 10 and 20 were utilized as thermal enhancement components within the absorber tubes of CPC. These tubes were designed to improve the heat transfer efficiency in descending order, starting at 3 cm, then 2 cm, and 1 cm in each of the two absorber tubes. Starting with the 3 cm insert, it provides a high heat transfer rate within the CPC absorber tube, enhancing the overall system efficiency. Moving on to the 2 cm insert, it allows further improvement in heat transfer, enabling more efficient thermal energy absorption. Finally, the 1 cm insert, the smallest size, provides a certain degree of thermal enhancement by augmenting the heat transfer area. In Figs. 8 (a) to (e), the impact of metal foam on hourly Nusselt number (Nu) is depicted for various flow rates, i.e., 0.2, 0.3, 0.4, 0.5, and 0.6 l/min, and different conditions, i.e., empty receiver, PPI10, and PPI20. Figs.8 (a) through (e) show time-dependent changes in Nu. The highest Nu values were observed in one of the CPC absorber tubes with Cu metal foam having a PPI of 20 (Fig. 8(a)) at 0.2 l/min around 11:30 PM, with an experimental Nu of 5.633 and a numerical Nu of 6.233. At 0.3 l/min (Fig. 8(b)) around 11:00 PM, Nu reached 7.179 experimentally and 7.979 numerically. Fig. 8(c) at 0.4 l/min (12:30 PM) recorded an experimental Nu of 8.809 and a numerical Nu of 7.979. At 0.5 l/min (Fig. 8(d), 12:30 PM), the experimental Nu was 8.403, while the numerical Nu was 8.903. Finally, at 0.6 l/min (Fig. 8(e), 12:30 PM), the experimental Nu reached 8.882, and the numerical Nu was 9.382. These findings indicate a substantial improvement in Nu with the inclusion of metal foam, suggesting its effectiveness as a heat transfer enhancement technique in the CPC system. Metal foam is a heat transfer enhancer due to its high surface area and porous structure. As the metal foam's PPI (pores per inch) increases from 10 to 20, there is a greater surface area for heat exchange, which enhances convective heat transfer and, consequently, increases the Nu number. The metal foam likely acts as an obstacle, facilitating better mixing of the working fluid within the absorber tube and increasing the heat transfer rate. However, the relatively lower Nu values suggest that there may still be room for optimization to operate the system at its maximum potential, particularly for PPI10. The same result was reported by [27].

5.2.2.Impact of Volume Flow Rate on the Hourly Nusselt Number

Figures 9 (a) to (c) illustrate the Nu number variations over time in solar collector tube receivers, comparing setups with different conditions (empty receiver, PPI10, and PPI20) for various flow rates (0.2, 0.3, 0.4, 0.5, and 0.6 l/min). It examines the influence of varying volume flow rates on hourly Nu during May and June. The data revealed how Nu changed throughout the day, shedding light on absorber tube performance. At 12:30 PM, the highest Nu values (7.937 experimentally, 8.437 numerically) were achieved at a flow rate of 0.6 l/min without metal foam (Baseline) in a CPC absorber tube. At 12:00 PM, another CPC absorber tube featuring Cu metal foam (PPI 10) reached its peak Nu values (8.456 experimentally, 8.856 numerically) at the same flow rate. At 11:30 PM, a CPC absorber tube with Cu metal foam (PPI 20) achieved the highest Nu values (8.882 experimentally, 9.382 numerically) at 0.6 l/min. Therefore, the Nu increased by approximately 4.95% for PPI10 and 11.22% for PPI20 compared to the baseline (without metal foam). The increase in Nu with higher flow rates is attributed to convective heat transfer principles. High flow rates result in more fluid passing through the collector pipe, raising the heat exchange between the HTF and absorber surface, which enhances the convective heat transfer coefficient, increasing Nu and improving the CPC thermal performance.

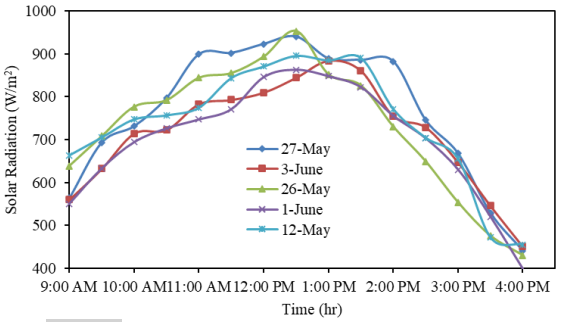

Fig. 6 Experimental Measurements for Concentrated Solar Irradiance Verses Time.

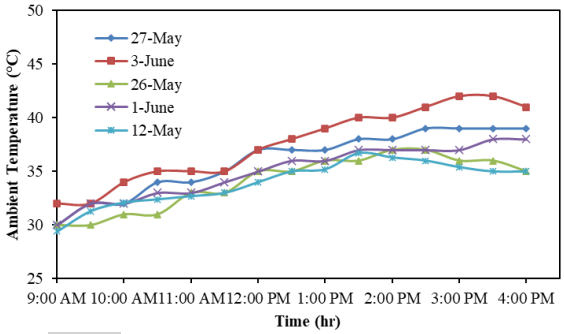

Fig. 7 Experimental Measurements for Ambient Temperatures Distribution Verses Time.

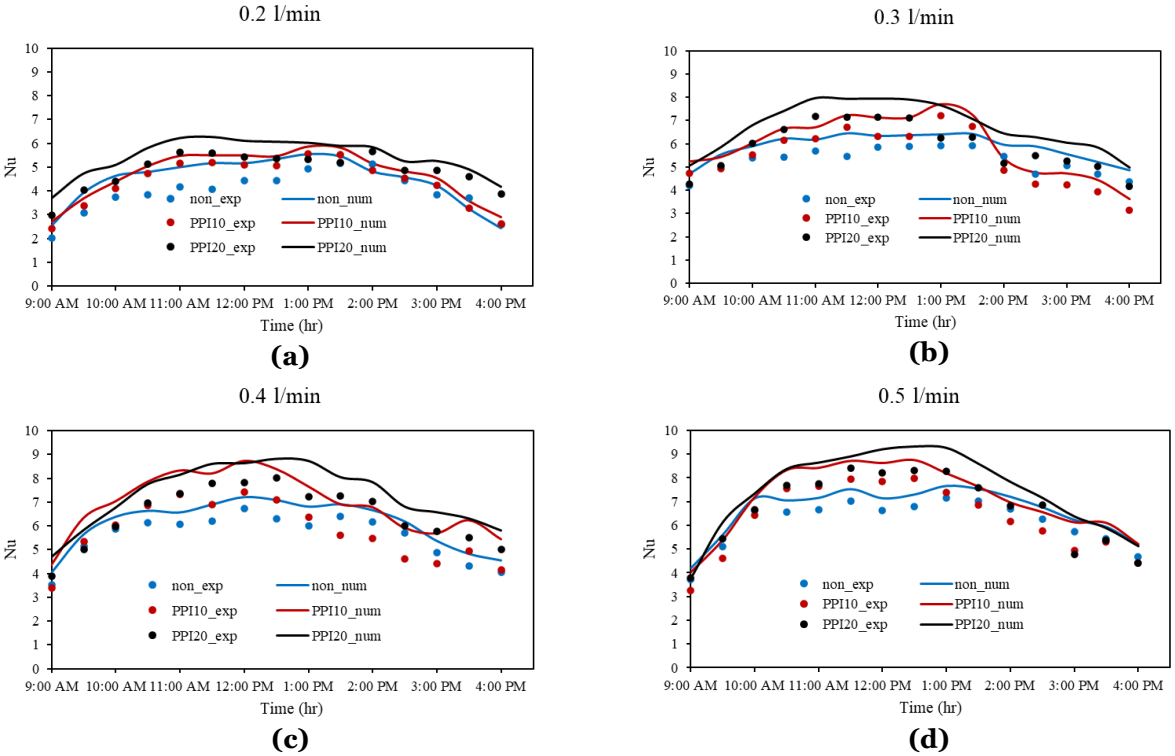

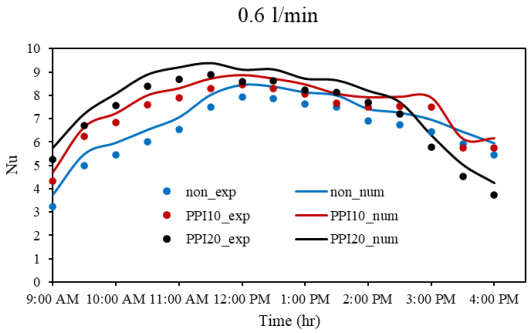

(e)

Fig. 8 Impact of Cu Metal Foam Inserts on Hourly Nu for Empty, PPI10, and PPI20 at (a) 0.2, (b) 0.3, (c) 0.4, (d) 0.5, and (e) 0.6 l/min.

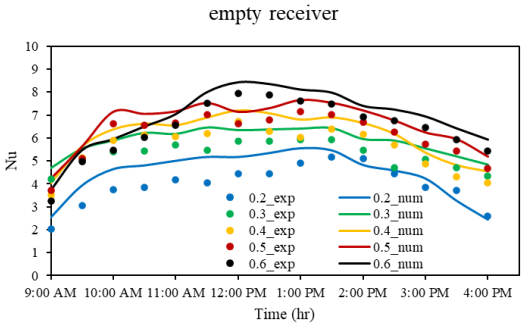

(a)

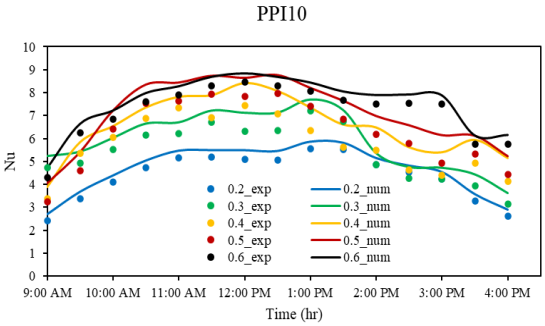

(b)

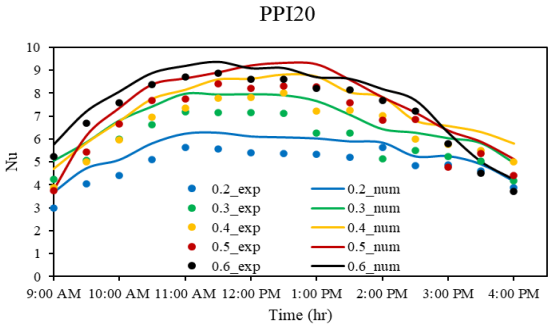

(c)

Fig. 9 Impact of Volume Flow Rates (l/min) on hourly Nusselt Number of Cu Metal Foam.

5.3.Thermal Efficiency

5.3.1.Impact of Metal Foam on the Hourly Thermal Efficiency

The thermal efficiency of a solar collector was examined under two distinct scenarios: one without the insertion of metal foam and the other with metal foam, with PPI10 and PPI20 configurations. These evaluations were conducted concerning varying solar radiation intensities. It is apparent from Figs. 11 (a) to (e) that as solar radiation intensity increased, the thermal efficiency of the collector also increased, especially when metal foam was inserted, as it enhanced heat retention and reduced heat losses. This observed behavior can be attributed to the continuous rise in the ambient temperature, reducing the collector's heat losses. In the absence of the metal foam, the maximum thermal efficiency was experimentally measured at 85%, while numerical simulations indicated a slightly higher value of 88%. This peak efficiency was observed at 01:30 PM. However, when copper (Cu) metal foam with a PPI10 configuration was inserted, the maximum thermal efficiency dropped to 81.87% experimentally and 82.82% numerically, occurring at 02:00 PM. Conversely, when Cu metal foam with a PPI20 configuration was inserted, there was a significant increase in the collector's maximum thermal efficiency. Experimentally, it reached 88.33%, and numerically, it reached 91.33%, both occurred at 01:30 PM. The percentage increase in thermal efficiency between the empty receiver, PPI10, and PPI20 configurations. Between the empty receiver and PPI10, there was an increase in thermal efficiency by approximately 3.13% experimentally and 5.18% numerically. Between PPI10 and PPI20, there was an increase in thermal efficiency by approximately 6.46% experimentally and 8.51% numerically. Similar conclusions were obtained by [28].

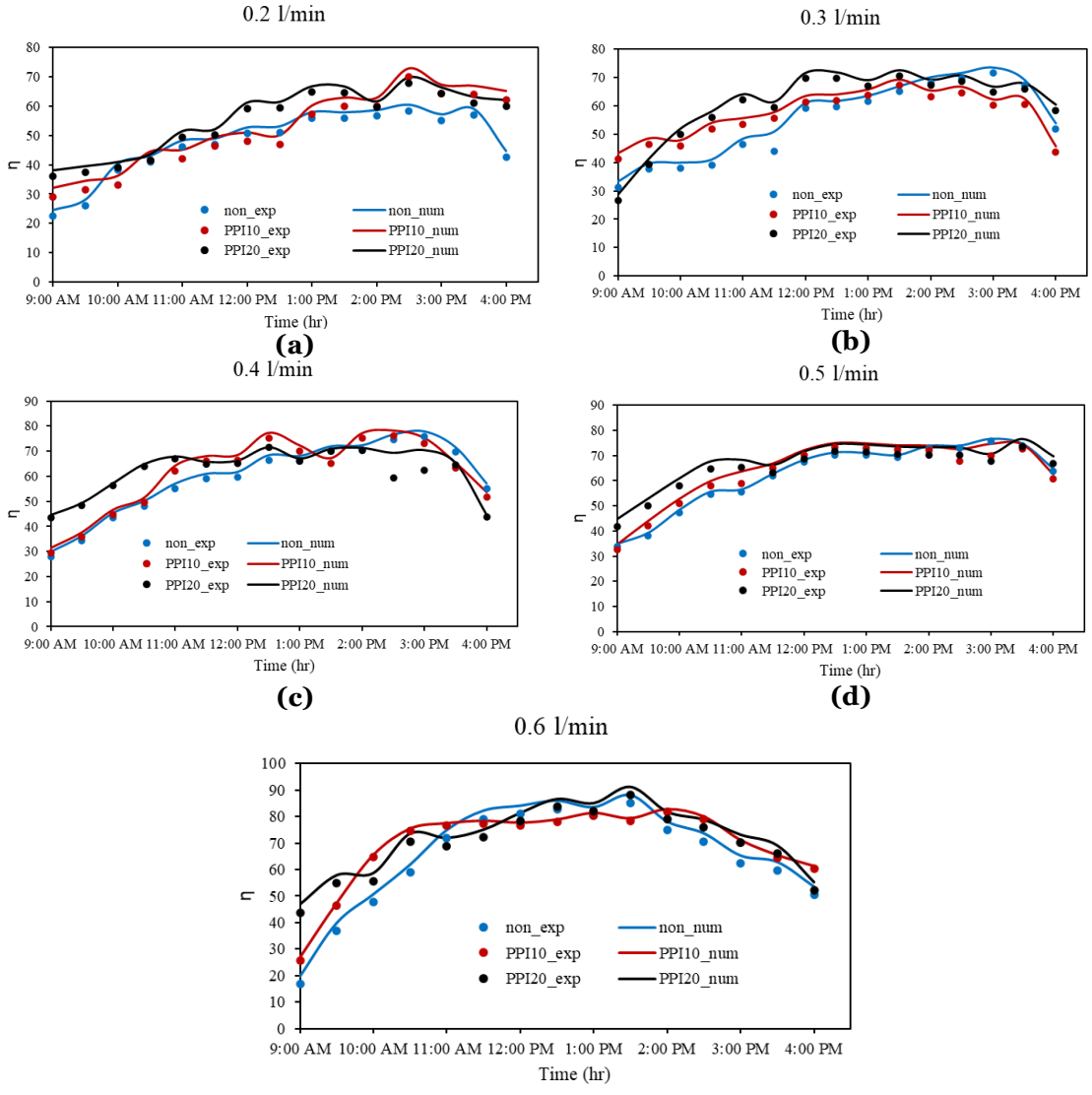

Fig. 10 Impact of Cu Metal Foam on Hourly Thermal Efficiency for Empty, PPI10, and PPI20 at (a) 0.2, (b) 0.3, (c) 0.4, (d) 0.5, and (e) 0.6 l/min.

5.3.2.Impact of Volume Flow Rate on the Hourly Thermal Efficiency

The thermal efficiency of the solar collector demonstrates an obvious pattern in Figs. 11(a) to (c), which depicted various flow rates (0.2, 0.3, 0.4, 0.5, and 0.6 l/min) and different conditions (empty receiver, PPI10, and PPI20), wherein it exhibits an upward trend in conjunction with a rise in solar radiation intensity. The observed behavior can be ascribed to the simultaneous rise in ambient temperature, resulting in decreased heat dissipation. Furthermore, a positive association exists between the collector's thermal efficiency and the water's volume flow rate through the collector. The primary reason for the observed gain in thermal efficiency is attributed to the reduction in the absorber tube temperature [16]. This decrease was crucial in minimizing heat losses from the collector to the surrounding environment. Furthermore, the thermal efficiency of the collector exhibited a significant enhancement when solar radiation intensity increased, mainly when the metal foam insertion was utilized. Metal foam improved heat retention and decreased heat losses, significantly contributing to the collector's overall efficiency. The improvement in the thermal efficiencies for both the empty receiver and the PPI20 receiver was as follows. At 1:30 PM, with a collector volume flow rate of 0.6 l/min, the empty receiver achieved a maximum thermal efficiency of 85%, while PPI20 reached 88.34%. Therefore, PPI20 exhibited a percentage increase in thermal efficiency of approximately 4.34% compared to the empty receiver under these conditions.

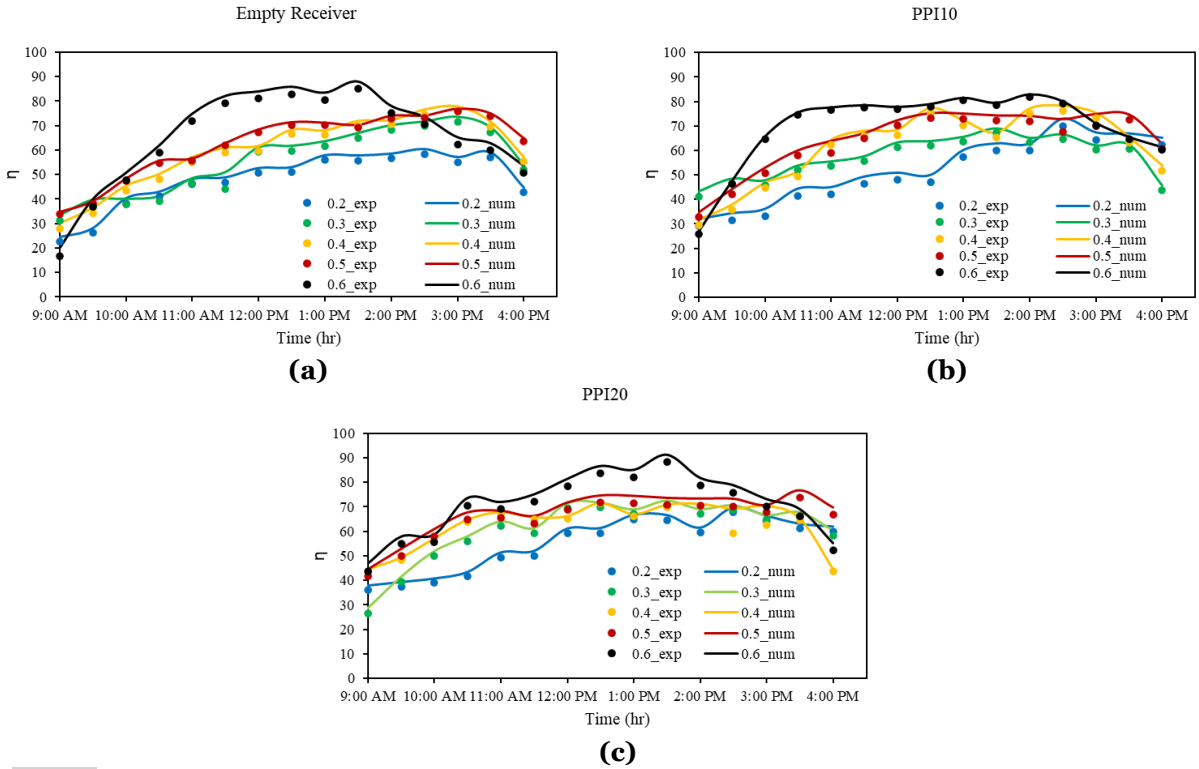

Fig. 11 Impact of Volume Flow Rate (l/min) on Hourly Thermal Efficiency (a) Empty Receiver, (b) PPI10, and (c) PPI20 at 0.2, 0.3, 0.4, 0.5, and 0.6 l/min.

5.4.Bulk Temperature Distribution

Figure 12 illustrates the impact of volume flow rate on the temperature distribution within a studied CPC receiver. This figure compares three insertions (empty, PPI10, and PPI20) and five volume flow rates (0.2 to 0.6 l/min) for Cu metal foam inserts at 12:00 PM. The results show that adding the metal foam inserts increased the bulk temperature along the receiver, enhancing the heat transfer from the receiver's surface to the heat transfer fluid (HTF). This heat transfer occurred through conduction within the receiver and convection from the metal foam to the HTF. Increasing the PPI from 10 to 20 also increased the bulk temperatures for all flow rates. Furthermore, higher HTF flow rates reduced the bulk temperatures because slower HTF allows more time to absorb heat from the receiver, resulting in higher temperatures. Conversely, faster HTF had less contact time with the hot receiver surface, leading to lower bulk temperatures. For example, with an empty receiver, mean bulk temperatures were reduced by 15% at 0.2 l/min and 6.4% at 0.6 l/min. For the Cu metal foam insertions, the reductions in mean bulk temperatures ranged from 2.5% to 9% for the PPI10 case and from 2.7% to 7.8% for the PPI20 case across the studied flow rates.

5.5.Water Outlet-Inlet Temperature Difference

Figure 13 shows the impact of inserting metal foam on the hourly water (flowing through the CPC receiver) outlet-inlet temperature at 0.2, 0.3, 0.4, 0.5, and 0.6 l/min. Throughout the test period, i.e., from 09:00 AM to 04:00 PM, the temperature difference followed the solar radiation intensity, i.e., it increased with the solar radiation and vice versa, for all studied cases. The receiver inserted with a metal foam produced a higher temperature difference for all studied volume flow rates than the empty. A similar result was reached by [15]. The highest temperature difference was indicated for PPI20 at 0.2 l/min and 01:00 PM, i.e., 23.3 K. PPI20 provides more contact area between the flowing water and the hot receiver surface, increasing the water temperature. Therefore, the water leaves the receiver with a higher temperature than the empty and PPI10 cases. In contrast, for 0.2 l/min, the highest temperature differences were 20.2 K and 21.5K at 01:30 for empty and PPI10 cases, respectively. For 0.3 l/min, the highest temperature differences were 15.1 K, 15.6 K, and 16.4 K at 01:30 PM for empty, PPI10, and PPI20, respectively. For 0.4 l/min, the highest temperature differences were 12.8 K, 13.8 K, and 14.5 K at 12:30 PM for empty, PPI10, and PPI20, respectively. For 0.5 l/min, the highest temperature differences were 9.8 K, 10.2 K, and 10.7 K at 12:30 PM for empty, PPI10, and PPI20, respectively. Finally, for 0.6 l/min, the highest temperature differences were 9.6 K, 10.2 K, and 10.6 K at 01:30 PM for empty, PPI10, and PPI20, respectively. The above data shows that the temperature difference decreased as the volume flow rate increased. The heat transfer time decreased as the water flow rate increased, reducing the water outlet temperature. As a result, the outlet-inlet temperature decreases.

5.6.Comparison with Previous Studies

Comparing the performance of the present system with other published studies is helpful to evaluate the suggested system. Table 4 shows a comparison between the present study's thermal efficiency and previous works. The comparison shows that the proposed system performed reasonably compared with other systems. Although the solar radiation of the present study was lower than other studies, the present high volume flow rate contributed to enhancing thermal efficiency. In addition, the gradual distribution of the metal foam inserts augmented the present thermal performance. The gradual distribution increased the HTF temperature with lower friction losses. Also, the receiver was enclosed in a well-insulated and evacuated wooden box.

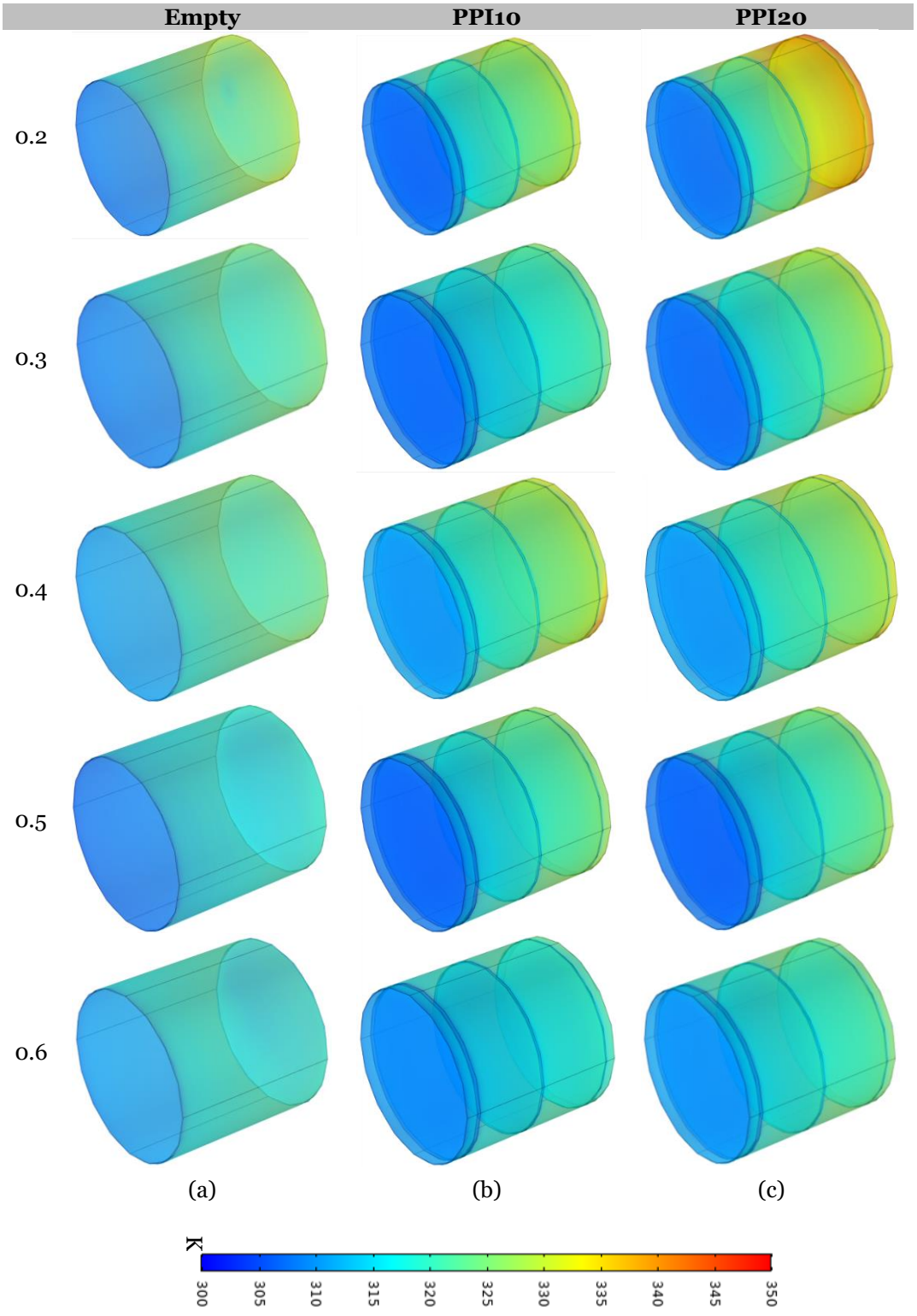

Fig. 12 Bulk Temperature Distribution for Cu Metal Foam Inserts (a) Empty, (b) PPI10, and (c) PPI20 at 0.2, 0.3, 0.4, 0.5, and 0.6 l/min at 12:00 PM.

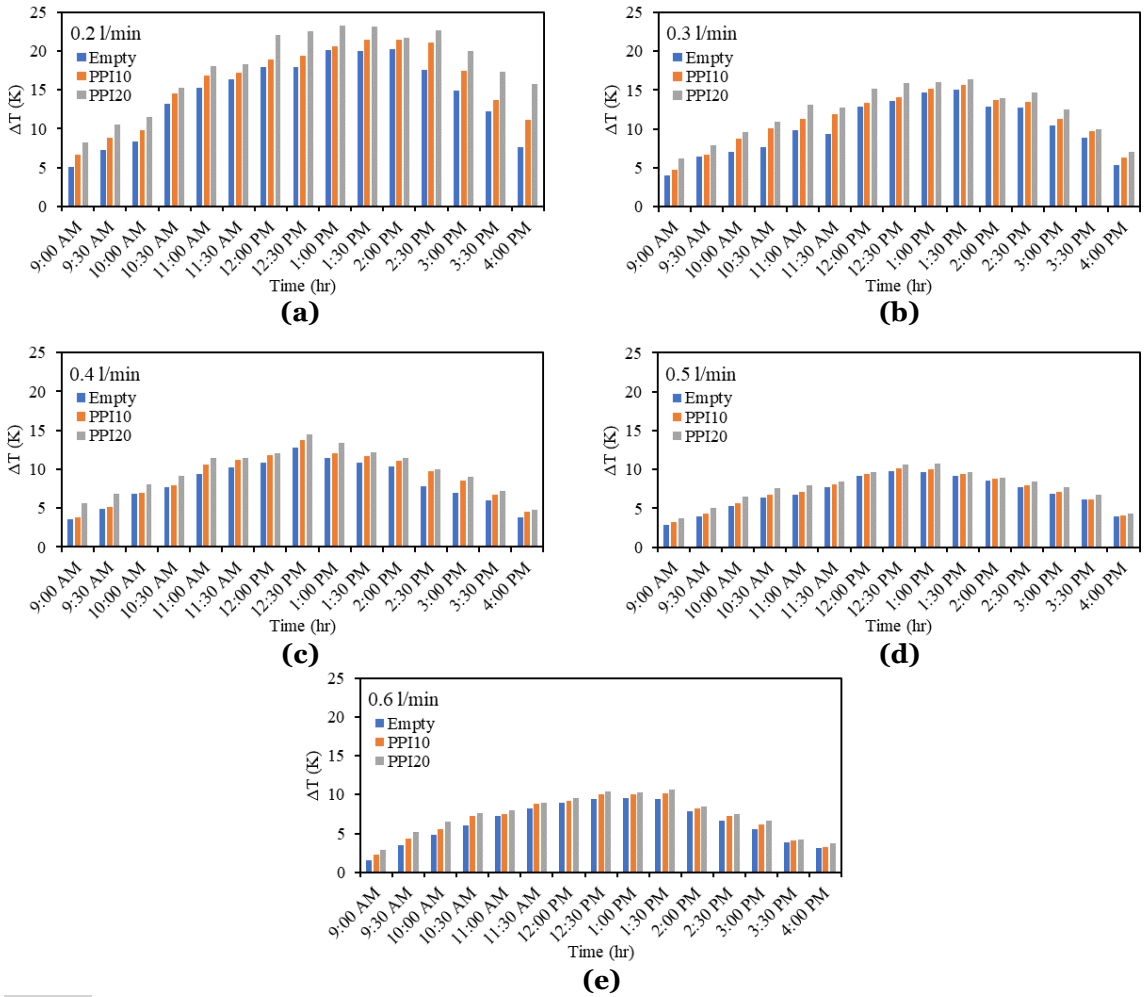

Fig. 13 Hourly Water Outlet-Inlet Temperature Difference for Cu Metal Foam Inserts for Empty, PPI10, and PPI20 at (a)0.2, (b) 0.3, (c) 0.4, (d) 0.5, and (e) 0.6 l/min.

Table 4 Comparison Between Previous Published Studies and the Present Study.

Reference	Collector type	HTF	η (%)	$\dot{V}$ (l/min)	Solar Radiation (W/m²)
Reddy et. al. [29]	Absorber tube with porous disc inserts	Water	69.0	4.48×10^{-3}	900
Kalidasan et. al. [30]	Absorber tube with hinged blade insert	Water	69.3	2.90×10^{-4}	950
Bellos et. al. [31]	Absorber tube with internal fins	Syltherm 800	68.5	4.14×10^{-2}	1000
Bellos et. al. [32]	Absorber tube with multiple cylindrical fins	Syltherm 800	68.1	2.77×10^{-2}	1000
Chakraborty et. al. [33]	PTC with helical absorber	Water	78.5	9.95×10^{-3}	708
Yılmaz et. al. [34]	PTC absorber with wire coil inserts	Therminol® Vp-1	76.5	1.99×10^{-1}	1000
Vengadesan et. al. [35]	PTC with semicircular structured thin flow absorber	Water	78.2	3.32×10^{-3}	975
Present study	CPC with gradual distributed metal foam inserts thickness (PPI20)	Water	67.1	0.3	884
	CPC with gradual distributed metal foam inserts thickness (PPI10)		63.7		884

6.CONCLUSIONS

The study conducted numerical simulations and experiments to assess how copper foam with consistent porosity and different PPI values (10 and 20) affected the novel compound parabolic solar collector receiver thermal performance. The focus was on mixed convection heat transfer in the absorber tubes, with tests conducted in Iraqi climate conditions and varying water flow rates. The key results are summarized below.

- Inserting Cu-foam improved the Nusselt number. For all studied volume flow rates, the receiver inserted with metal foam resulted in a higher Nusselt number. For instance, at 0.4 l/min, compared to the empty receiver, the Nusselt number improved by 3% experimentally and 13.3% numerically for the Cu-PPI10. For Cu-PPI20, the improvement in Nu was 15.7% experimentally and 19.1% numerically. Also, the results above showed that a higher PPI resulted in a better Nusselt number.
- The thermal efficiency was enhanced by inserting Cu-foam. Compared to the empty receiver at 0.2 l/min, the thermal efficiency

improved by 7.4% experimentally and 9.1% numerically by inserting PPI10 and 15.7% experimentally and 15.0% numerically by inserting PPI20.

- The difference in heat transfer fluid outlet-inlet temperature increased due to adding Cu-foam inserts. At 0.2 l/min, the Cu-foam-PPI10 temperature difference was 6.4% higher than the empty receiver, and the Cu-foam-PPI20 temperature difference was 15.3% higher than the empty receiver.
- As a future work, the impact of the metal foam insert thickness and location on the CPC receiver performance can be investigated.

NOMENCLATURE

D_h	The receiver hydraulic diameter, m
A_a	Aperture Area, m²
A_p	Area of absorber tube receiver, m²
U_L	Overall heat loss coefficient, W/m² K
h_z	The local convection heat transfer coefficient, W/m² K
T_r	The receiver temperature, K
T_a	The air temperature, K
T_o	The leaving water temperature, K
T_i	The entering water temperature, K
T_m	The water mean temperature, K
S	The absorbed radiation, W/m²
G_t	The total incident radiation on the aperture plane, W/m²
n	The average number of reflections
F'	The collector efficiency factor
$\dot{m}$	Mass flow rate, kg/s
c_p	The specific heat of water, J/kg K
Q_u	The useful energy gain, W
k	The heat fluid thermal conductivity, W/m K
Nu	Nusselt number
Greek Symbols	
τ_g	Transmissivity of the cover glazing
α_r	Absorptivity of receiver
τ_{CPC}	Effective transmissivity of CPC
ρ	The reflector reflectivity
η	The collector efficiency
ν	Kinematic viscosity, m²/s
α	Heat diffusivity, m²/s
μ	Dynamic viscosity, kg/ m s
ε	Porosity
Subscripts	
a	aperture
CPC	Compound Parabolic Collector
eff	effective
g	Glass cover
in	inlet
m	mean
out	outlet
r	receiver
th	thermal
u	useful

REFERENCES

[1] Mohtasham J. **Review Article-Renewable Energies**. *Energy Procedia* 2015; **74**:1289–1297.

[2] Behar O, Khellaf A, Mohammedi K. **A Review of Studies on Central Receiver Solar Thermal Power Plants**. *Renewable and Sustainable Energy Reviews* 2013; **23**:12–39.

[3] Dheyab HS, Al-Jethelah M, Ibrahim TK, Sirine Chtourou, Mounir Baccar. **Closed Solar Air Heater System Integrated with PCM (RT42 and RT50) in a Thermal Storage-Finned Heat Exchanger Unit**. *Tikrit Journal of Engineering Sciences* 2023; **30**(3):27–37.

[4] Al-Jethelah MSM. Thermal Energy Storage for Solar Energy Applications Based on Regular and Composite Nano-Phase Change Materials. PhD, University of Guelph, 2018.

[5] Mohammed GA, Mohammed ZS. **Modeling Horizontal Single Axis Solar Tracker Upon Sun-Earth Geometric Relationships**. *Tikrit Journal of Engineering Sciences* 2022; **29**(3):43–48.

[6] Tian Y, Zhao CY. **A Review of Solar Collectors and Thermal Energy Storage in Solar Thermal Applications**. *Applied Energy* 2013; **104**:538–553.

[7] Alami AH, Olabi AG, Mdallal A, Rezk A, Radwan A, Rahman SMA, et al. **Concentrating Solar Power (CSP) Technologies: Status and Analysis**. *International Journal of Thermofluids* 2023; **18**:100340, (1-24).

[8] Bellos E, Tzivanidis C. **A Review of Concentrating Solar Thermal Collectors with and without Nanofluids**. *Journal of Thermal Analysis and Calorimetry* 2019; **135**(1):763–786.

[9] Chen K, Guo L, Wang H. **A Review on Thermal Application of Metal Foam**. *Science China Technological Sciences* 2020;**63**(12):2469–2490.

[10] Duan R. **The Efficiency of New Solar Flat-Plate Collector**. *Advanced Materials Research* 2011;**347–353**:1337–1341.

[11] Wang P, Liu DY, Xu C. **Numerical Study of Heat Transfer Enhancement in the Receiver Tube of Direct Steam Generation with Parabolic Trough by Inserting Metal Foams**. *Applied Energy* 2013; **102**:449–460.

[12] Ali RMK, Lafta Ghashim S. **Numerical Analysis of the Heat Transfer Enhancement by Using Metal Foam**. *Case Studies in Thermal Engineering* 2023; **49**:103336, (1-16).

[13] Albojamal A, Haghighi A, Hamzah H. **Analysis of Thermal Transport Through a Flat-Plate Solar Collector Integrated with Metal-Foam Blocks**. *The International Journal of Energy and Engineering Sciences* 2017; **2**(2): 55-68.

[14] Ranjithkumar K, Pradeep Kumar SL, Jayaprakash L. **Design and Thermal**

Analysis of Solar Plate Collector with and without Porous Medium. *International Journal of Innovative Research in Science Engineering and Technology* 2015; **4**:447–457.

[15] Jamal-Abad MT, Saedodina S, Aminy M. **Experimental Investigation on the Effect of Partially Metal Foam inside the Absorber of Parabolic Trough Solar Collector**. *International Journal of Engineering* 2017; **30**(2): 281-287.

[16] Valizade M, Heyhat MM, Maerefat M. **Experimental Study of the Thermal Behavior of Direct Absorption Parabolic Trough Collector by Applying Copper Metal Foam as Volumetric Solar Absorption**. *Renewable Energy* 2020; **145**:261–269.

[17] Heyhat MM, Zahi Khattar M. **On the Effect of Different Placement Schemes of Metal Foam as Volumetric Absorber on the Thermal Performance of a Direct Absorption Parabolic Trough Solar Collector**. *Energy* 2023; **266**:126428.

[18] Saedodin S, Zamzamian SAH, Nimvari ME, Wongwises S, Jouybari HJ. **Performance Evaluation of a Flat-Plate Solar Collector Filled with Porous Metal Foam: Experimental and Numerical Analysis**. *Energy Conversion and Management* 2017; **153**:278–287.

[19] Peng H, Li M, Hu F, Feng S. **Performance Analysis of Absorber Tube in Parabolic Trough Solar Collector Inserted with Semi-Annular and Fin Shape Metal Foam Hybrid Structure**. *Case Studies in Thermal Engineering* 2021; **26**:101112, (1-15).

[20] Brodkey RS, Hershey HC. Transport Phenomena: A Unified Approach, 1988.

[21] Aleshkova IA, Sheremet MA. **Unsteady Conjugate Natural Convection in a Square Enclosure Filled with a Porous Medium**. *International Journal of Heat and Mass Transfer* 2010; **53**(23–24):5308–5320.

[22] Sankar M, Park Y, Lopez JM, Do Y. **Numerical Study of Natural Convection in a Vertical Porous Annulus with Discrete Heating**. *International Journal of Heat and Mass Transfer* 2011; **54**(7–8):1493–1505.

[23] Akbarzadeh M, Rashidi S, Keshmiri A, Shokri N. **The Optimum Position of Porous Insert for a Double-Pipe Heat Exchanger Based on Entropy Generation and Thermal Analysis**. *Journal of Thermal Analysis and Calorimetry* 2020;**139**(1):411–426.

[24] Nield DA, Bejan A. Convection in Porous Media. Cham: Springer International Publishing.

[25] Kalogirou S. Solar Energy Engineering: Processes and Systems. Burlington, MA: Elsevier/Academic Press, 2017.

[26] Moffat RJ. **Describing the Uncertainties in Experimental Results**. *Experimental Thermal and Fluid Science* 1988; **1**(1):3–17.

[27] Kurtbas I, Celik N. **Experimental Investigation of Forced and Mixed Convection Heat Transfer in a Foam-Filled Horizontal Rectangular Channel**. *International Journal of Heat and Mass Transfer* 2009; **52**(5–6):1313–1325.

[28] Jamal-Abad MT, Saedodin S, Aminy M. **Experimental Investigation on a Solar Parabolic Trough Collector for Absorber Tube Filled with Porous Media**. *Renewable Energy* 2017; **107**:156–163.

[29] Ravi Kumar K, Reddy KS. **Thermal analysis of solar parabolic trough with porous disc receiver**. *Applied Energy* 2009;**86**(9):1804–1812.

[30] Kalidasan B, Shankar R, Srinivas T. **Absorber Tube with Internal Hinged Blades for Solar Parabolic Trough Collector**. *Energy Procedia* 2016; **90**:463–469.

[31] Bellos E, Tzivanidis C, Tsimpoukis D. **Optimum Number of Internal Fins in Parabolic Trough Collectors**. *Applied Thermal Engineering* 2018; **137**:669–677.

[32] Bellos E, Daniil I, Tzivanidis C. **Multiple Cylindrical Inserts for Parabolic Trough Solar Collector**. *Applied Thermal Engineering* 2018; **143**:80–89.

[33] Chakraborty O, Roy S, Das B, Gupta R. **Effects of Helical Absorber Tube on the Energy and Exergy Analysis of Parabolic Solar Trough Collector – A Computational Analysis**. *Sustainable Energy Technologies and Assessments* 2021; **44**:101083.

[34] Yılmaz İH, Mwesigye A, Göksu TT. **Enhancing the Overall Thermal Performance of a Large Aperture Parabolic Trough Solar Collector Using Wire Coil Inserts**. *Sustainable Energy Technologies and Assessments* 2020; **39**:100696.

[35] Vengadesan E, Ismail Rumaney AR, Mitra R, Harichandan S, Senthil R. **Heat Transfer Enhancement of a Parabolic Trough Solar Collector Using a Semicircular Multitube Absorber**. *Renewable Energy* 2022; **196**:111–124.